A Physiochemical Processing Kinetics Model for the Vapor Phase Infiltration of Polymers: Measuring the Energetics of Precursor-Polymer Sorption, Diffusion, and Reaction

Journal:	*Physical Chemistry Chemical Physics*
Manuscript ID	CP-ART-06-2018-004135.R1
Article Type:	Paper
Date Submitted by the Author:	26-Jul-2018
Complete List of Authors:	Leng, Collen; Georgia Institute of Technology, Materials Science and Engineering Losego, Mark; Georgia Institute of Technology, Materials Science and Engineering

PCCP

PAPER

A Physiochemical Processing Kinetics Model for the Vapor Phase Infiltration of Polymers: Measuring the Energetics of Precursor-Polymer Sorption, Diffusion, and Reaction

Received 00th January 20xx,
Accepted 00th January 20xx

DOI: 10.1039/x0xx00000x

www.rsc.org/

Collen Z. Leng [a] and Mark D. Losego*[a]

Vapor phase infiltration (VPI) is a new approach for transforming polymers into organic-inorganic hybrid materials with unique properties. Here, we combine experimental measurements with phenomenological theory to develop a universal strategy for measuring, modeling, and predicting the processing kinetics of VPI. We apply our approach to the well-studied VPI system of trimethylaluminum (TMA) infiltrating poly(methyl methacrylate) (PMMA) because the system undergoes both precursor-polymer diffusion and reaction. By experimentally measuring aluminum concentration profiles as a function of film depth with secondary ion mass spectrometry (SIMS) and film swelling with ellipsometry, we have extracted equilibrium solubility and effective diffusivity as a function of process temperature. Fitting these values to appropriate Van't Hoff and Arrhenius relationships, we can then extract enthalpies for precursor sorption and diffusion. We observe an abrupt mechanistic change in both the sorption and diffusion processes around 95 °C, where greater chain mobility at higher processing temperatures lead to greater reactivity between TMA and PMMA. With new understanding of this VPI process, we demonstrate precise control of inorganic infiltration depth and loading fraction into PMMA.

1. Introduction:

Organic-inorganic hybrid materials can merge properties normally exclusive to either the pure organic or inorganic component. Hybrid materials are most commonly synthesized via liquid solution processing. However, solution processing can be synthetically complex and difficult to form into arbitrary geometric form factors. Vapor phase infiltration (VPI) is a new method that uses gaseous precursors to transform polymers into organic-inorganic hybrid materials.[1-11] In VPI, an organic polymer is exposed to metalorganic vapors that infiltrate into and potentially react with the polymer. VPI has been used to create stronger natural fibers,[3] increase charge collection in hybrid photovoltaics,[5] alter the fluorescence of polymers,[10] act as contrasting agents for imaging of copolymer structures,[12] improve etch resistance in lithographic patterning,[13] enhance doping in conductive polymers for flexible electronics,[14] create novel triboelectric energy generators,[15] and serve as anti-reflection coatings.[16]

Maximizing infiltration depth can expand the application space for VPI created hybrid materials beyond thin films to polymeric sheets, foams, and textiles. For example, infiltrated foams have been demonstrated to be more effective oil sorbents.[17] Understanding the fundamental kinetics (sorption, diffusion, and reaction) of the VPI process is critical to maximizing and rationally designing the infiltration depth and inorganic loading fraction. While much is known about small molecule sorption and diffusion in polymers as it relates to membranes for chemical separations,[18-22] far fewer studies exist about the fundamental thermodynamics and kinetics of metalorganic vapor species—needed for VPI—permeating and reacting with polymers. In 2007 Sinha *et al.* reported on the sorption enthalpy and diffusivity of several titanium metalorganic precursors in polymeric photoresists[23] and in 2017 Peng *et al*. reported on the diffusivity of $TiCl_4$ in several polymers at a fixed process temperature.[24] However, the VPI process has yet to receive a careful, holistic theoretical and experimental treatment of its relevant thermodynamic and kinetic processing parameters. In this paper, we use a simple, single dose-and-hold process to study the infiltration kinetics of trimethylaluminum (TMA) infiltrated into poly(methyl methacrylate) (PMMA) thin films on impermeable substrates (silicon wafers). Using the Van't Hoff equation for reaction equilibrium and Fick's 2nd law of diffusion, we extract equilibrium solubilities and effective diffusion coefficients and, ultimately, fundamental enthalpies for the sorption, diffusion, and reaction processes occurring during VPI. Using these measured values, we then demonstrate our ability to use this theory for rational materials design by infiltrating a PMMA film to an arbitrarily specified depth.

[a] School of Materials Science and Engineering, Georgia Institute of Technology, 771 Ferst Drive NW, Atlanta, GA 30332, USA. *E-mail: losego@gatech.edu
[b] Electronic Supplementary Information (ESI) available: See DOI: 10.1039/x0xx00000x

2. Experimental Methods:

Spun-cast PMMA films on silicon substrates infiltrated with TMA are selected as a prototypical system to study the 1-dimensional VPI processing kinetics. PMMA films (MW = 15 kDa, T_g = 105 °C, Sigma-Aldrich) were spun-cast from solutions of toluene (for thinner films of < 200 nm) or cyclohexanone (for thicker films of > 200 nm). Spin-casting at 3000 rpm for 60 s from toluene (2 wt% to 6 wt% PMMA) gave films ranging in thickness from 50 nm to 200 nm. Higher concentrations of PMMA could be dissolved in cyclohexanone (up to 20 wt%). These solutions were used to prepare thicker PMMA films up to 2 µm. After spin coating, films were placed in a vacuum oven at 160° C for ≥ 1 hour to remove the solvent and relax the polymer. This annealing step reduces film thickness by about 10% from the original spun-cast state.

VPI was performed in a custom-built vapor phase reactor specifically designed for infiltration (Figure 1). Two gate valves are incorporated to permit isolation of the reaction chamber in a static VPI atmosphere. By connecting VPI precursors directly to the static reactor, we can better control dosing time and vapor concentration, enabling more fundamental studies of the processing kinetics. Single dose infiltration tests of TMA into PMMA were carried out over a temperature range of 60 °C to 130 °C and at exposure times ranging from 1 second to 1000 minutes. (**NOTE**: ***TMA is pyrophoric and must be handled with caution***.) This processing temperature range covers the glass transition temperature (T_g = 105 °C) of pure PMMA. Before each infiltration test, the samples were purged with ultra-high purity N_2 for 5 minutes at 150 sccm inside the VPI reactor to allow adequate removal of water and other impurities. The reactor was then pumped down to base pressure (~20 mTorr) for 2 minutes before the two gate valves were closed to isolate the chamber. TMA is then dosed for 1 second directly into the chamber through a diaphragm valve to a pressure of approximately 0.5 Torr. TMA infiltrates the PMMA films for a predetermined time before the gate vales are re-opened and the chamber is purged with about 2 Torr of N_2 for 60 s followed by a 1 s water dose to react with any residual TMA within the film or inside the chamber. We assume that once the material is exposed to water, all TMA becomes trapped within the PMMA film (no further desorption).

Aluminum concentration depth profiles of the infiltrated PMMA films were measured with time-of-flight secondary ion mass spectrometry (ToF-SIMS, IONTOF, 5 Series). For simplicity, only infiltration profiles that could be fit to a semi-infinite diffusion model were evaluated; in other words, no diffusion profile was permitted to reach the substrate in these SIMS studies. To accommodate this constraint, thicker films (~1.4 microns) or shorter infiltration times were used. SIMS spectra were collected using oxygen sputtering (150 µm x 150 µm) and bismuth analyzer beams (50 µm x 50 µm). Positive polarity was used to detect the Al+ signal from infiltrated TMA. Sputter rates were calculated from profilometry measurements of final crater depths (see supplementary information for additional details).

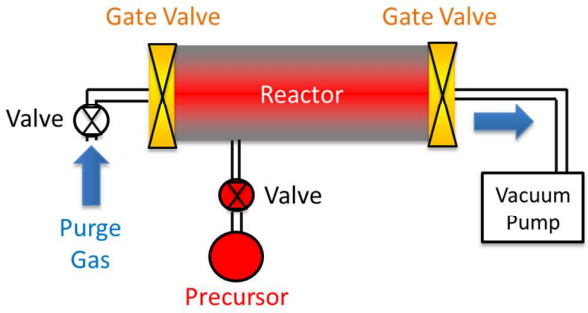

Figure 1: *Basic schematic of our custom-built VPI reactor.*

Diffusional data was also collected from film swelling. Swelling was measured *ex situ* with spectroscopic ellipsometry (Woollam Alpha-SE). These swollen thicknesses were used as a proxy for total mass uptake by the polymer as a function of time. To measure infiltrated thickness with ellipsometry, films were modeled as a single homogeneous layer with some allowance for adjusting refractive index away from that of pure PMMA to achieve mean square error (MSE) values below 5 for most samples. Ellipsometry models that included roughness and/or graded layers showed no significant improvements in data fitting or changes in layer thickness since the refractive indices of pure PMMA and amorphous aluminum oxide are within 10% of one another. Because infiltration rate increases with higher temperature, films of different thicknesses were used across the temperature range. This ensures that films can reach maximum swelling within reasonable times without saturating too quickly. To achieve sufficient temporal resolution for the diffusion process, PMMA films of about 150 nm thick were used for process temperatures lower than 100 °C, and 500 nm thick films were used for process temperatures above 100 °C.

Fourier transform infrared spectroscopy (FTIR, Thermo Scientific, Nicolet iS5) with a germanium ATR crystal was used to characterize changes within the PMMA chemistry due to VPI processing. To avoid signal interference from the silicon substrate, 1.4 micron thick PMMA films were used for these measurements.

Cross sections of infiltrated films were visualized with a Hitachi SU8230 SEM with EDX. To prepare cross sections, films on pieces of single crystal silicon wafers were broken in half via a small crack initiated from a diamond scribe. These fractured pieces were then attached with carbon tape to vertical SEM stubs. Approximately 10 nm of carbon was sputtered onto the cross-section to prevent charging but not block the EDX signal. SEM images were taken at an accelerating voltage of 0.5 kV. EDX was taken using an accelerating voltage of 4 kV to reduce film damage but provide sufficient energy to emit characteristic K-shell x-rays from the aluminum atoms (~1.5 keV).

3. Phenomenological Model for Vapor Phase Infiltration (VPI) Kinetics:

Vapor phase infiltration is a three step process: 1) metalorganic gases sorb into the polymer, 2) these sorbed gases become "penetrants" that diffuse within the polymer, and 3) these penetrants become entrapped within the polymer via either reaction or other mechanism (e.g., steric hindrance or loss of volatility).[1] Figure 2 schematically depicts these processes.

The first step of the VPI process is sorption of the vapor phase molecular precursor into the polymer. Thermodynamically, the concentration (C) of a penetrant (precursor) molecule in a polymer depends upon the partial pressure (P) of that penetrant species and the solubility coefficient (S), via: C = SP (Henry's Law). Here we assume that the low pressures of VPI (< 1 Torr) keep the system sufficiently dilute that Henry's Law is sufficient to describe the sorption equilibrium. Because S is essentially the equilibrium reaction constant for sorption, it scales exponentially with temperature (T) according to the Van't Hoff relationship:

$$S = S_o \exp\left(-\frac{\Delta H_s}{kT}\right) \quad \textbf{Equation 1}$$

where S_o is a temperature-independent constant based upon the change in entropy for this reaction, k is Boltzmann's constant, and ΔH_S is the enthalpy of sorption. Thus, when the natural log of the solubility coefficient is plotted versus the inverse of absolute temperature, the slope of this line is proportional to ΔH_S. The maximum solubility at a given temperature can be used in subsequent diffusion calculations as the "maximum concentration" (C_{max}) of source precursor at the polymer surface and can also be related to the total mass uptake at infinite time, M_∞ (*vide infra*).

The second step in VPI, precursor diffusion, can be described by Fick's 2nd Law for time-dependent diffusion:

$$\frac{\partial C}{\partial t} = D\frac{\partial^2 C}{\partial x^2} \quad \textbf{Equation 2}$$

where D is the diffusion coefficient, x is the distance into the film, and t is time. For our experiments, we solve this equation for the case of 1-dimensional diffusion into a film with an impermeable substrate.[1] However, once the diffusional activation energy is measured, Fick's 2nd Law can readily be solved for any diffusional geometry.[25] The boundary conditions for a film on substrate include constant precursor concentration at the free polymer surface (C_{max}) and zero flux at the film/substrate interface. Solving Fick's 2nd Law under these constraints yields:

$$C(x,t) = C_{max}\left(1 - \sum_{n=0}^{\infty}\frac{2}{\lambda_n}\sin\left(\frac{\lambda_n x}{L}\right)e^{-\frac{D\lambda_n^2 t}{L^2}}\right) \quad \textbf{Equation 3}$$

where

$$\lambda_n = \frac{(2n+1)\pi}{2}, n = 0, 1, 2, \ldots \quad \textbf{Equation 4}$$

and L is the film thickness. Integrating this equation over the entire film thickness yields the total mass uptake as a function of time (M_t). This equation can then be normalized to the total mass uptake at infinite time (M_∞):

$$\frac{M_t}{M_\infty} = 1 - \sum_{n=0}^{\infty}\frac{2}{\lambda_n^2}e^{-\frac{D\lambda_n^2 t}{L^2}}. \quad \textbf{Equation 5}$$

Both Equations 3 and 5 can be fit to experimental data to extract diffusivity. Equation 3 is appropriate when penetrant concentration is measured as a function of diffusion depth (e.g., with secondary ion mass spectrometry) while Equation 5 is appropriate when total penetrant concentration is measured as a function of infiltration time (e.g., with film swelling or gravimetry). When Equation 5 is plotted as a function of the square root of time, the initial linear slope approximates diffusivity through the following relationship:

$$\frac{\frac{M_t}{M_\infty}}{\sqrt{t}} = \frac{2}{L}\left(\frac{D}{\pi}\right)^{\frac{1}{2}}. \quad \textbf{Equation 6}$$

Being a thermally activated process, diffusivity can be fit to an Arrhenius relationship:

$$D = D_o \exp\left(-\frac{\Delta H_D}{kT}\right) \quad \textbf{Equation 7}$$

where ΔH_D is the activation energy for diffusion and D_o depends on the vibrational frequency of attempts for a penetrant to make a single diffusional hop. Therefore, temperature dependent measurements of diffusivity can be used to extract the activation energy for diffusion (ΔH_D).

Finally, VPI precursors may also react with their host polymer. For example, *in situ* FTIR studies of TMA VPI of PMMA have revealed reactions between the penetrants and the polymer's carbonyl groups.[26-28] These reactions can act as a "sink" for the diffusing penetrants, reducing the unreacted precursor's effective concentration in the polymer. Depending on the reaction rate, this "sink" for penetrants may resemble an increase in diffusional activation energy because penetrants become "trapped" at reaction sites rather than diffusing deeper into the material. At these higher reaction rates, we can assume a local equilibrium in the material that follows a "reaction sink": $(\partial C^*/\partial t)$, where C* is the concentration of

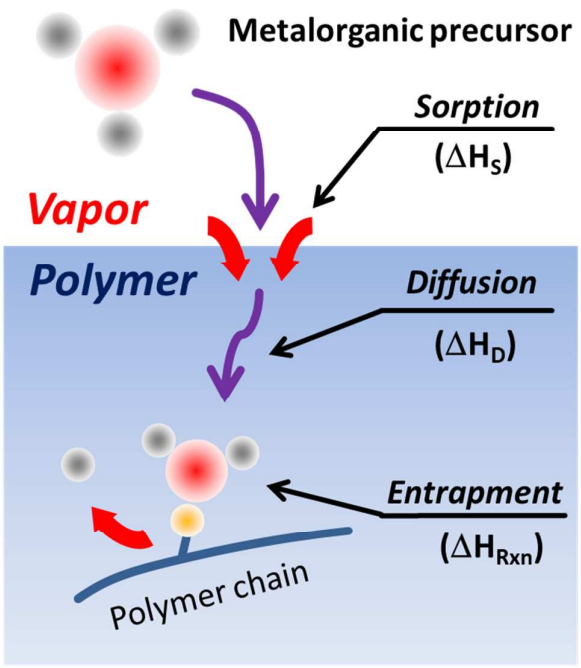

Figure 2: *Schematic for the atomic scale mechanisms occurring during vapor phase infiltration.*

precursors that have reacted with the polymer. Assuming a first order immobilization rate the reaction constant (K) can be written as:

$$K = \frac{C^*}{C} \qquad \textbf{Equation 8}$$

This reaction rate can then be added to Fick's 2nd Law:

$$\frac{\partial C}{\partial t} = D\frac{\partial^2 C}{\partial x^2} - \frac{\partial C^*}{\partial t} \qquad \textbf{Equation 9}$$

which by combining with Equation 8 can be algebraically simplified to:

$$\frac{\partial C}{\partial t} = \frac{D}{K+1}\frac{\partial^2 C}{\partial x^2}, \qquad \textbf{Equation 10}$$

This solution implies that with reactions, an "effective diffusion coefficient" (D^*) can be defined as:

$$D^* = \frac{D}{K+1}. \qquad \textbf{Equation 11}$$

Thus, the solution to Fick's 2nd Law with a reaction sink will have the same functional form as pure diffusion, except the diffusion coefficient will be convolved with the reaction equilibrium constant. As a consequence, diffusion will appear to be slower because the diffusion flux is effectively reduced by reactive consumption of penetrant molecules. Here, we note that reactions between precursors and polymer can create a new material with a high concentration of reacted species. This new material may have a much different diffusion coefficient than the original polymer, turning D into a function of C and complicating the diffusion model. In this situation, D can either be approximated, or a more complex numerical solution may be required.

Two extreme cases exist for D*: (1) when the reaction constant is small (K << 1), penetrants will freely diffuse with minimal influence from reactions, and (2) when the reaction constant is large (K >> 1), reactions will immobilize most penetrants, thereby effectively determining the transport rate. For the former case (K << 1), D^* reduces to D, suggesting that reaction kinetics are "inconsequential" to the total process kinetics. In the latter case (K >> 1), Equation 11, can be rewritten as:

$$D^* = \frac{D}{K} \qquad \textbf{Equation 12}$$

A Van't Hoff equation can then be used to describe the temperature dependence of the reaction equilibrium:

$$K = K_o exp\left(\frac{-\Delta H_{rxn}}{kT}\right). \qquad \textbf{Equation 13}$$

where K_o includes the temperature independent entropy change for the reaction. Substituting the temperature dependent reaction (Equation 13) and diffusion (Equation 7) equations into Equation 12, it is possible to write a new Arrhenius-like expression for the effective diffusion coefficient with reaction:

$$D^* = D_0^* \exp\left(-\frac{\Delta H_D - \Delta H_{rxn}}{kT}\right) \qquad \textbf{Equation 14}$$

where ΔH_{rxn} is the reaction enthalpy for the precursor-polymer reaction, D_o^* is a temperature-independent term that combines phenomena related to the entropy of reaction and the attempt frequency for diffusional hopping into a new constant. Assuming the reaction is exothermic (favorable), ΔH_{rxn} would be a negative value and additive with ΔH_D, creating a larger "effective" barrier to diffusion, effectively slowing the diffusion rate.

4. Results:

Figure 3 shows representative data illustrating our approach for extracting diffusion and solubility coefficients from SIMS depth concentration data and film swelling profiles. Figure 3a is a representative SIMS depth profile for an 80 nm PMMA film partially infiltrated with TMA for 10 s at 70 °C. Figure 3b fits this SIMS profile to Equation 3 (dotted line) to extract an effective diffusion coefficient of the TMA penetrant in PMMA of $2.2\text{x}10^{-14}$ cm^2/s. The process for calibrating and appropriately normalizing the SIMS signal to achieve this fit is detailed in the SI.

Figure 3c plots the PMMA film thickness (measured with ellipsometry) after VPI of various process times at the same process temperature (70 °C). We assume that film swelling is a reasonable proxy for the total mass uptake in the film as a function of VPI process time. Since each infiltrated film is purged with nitrogen for 60 seconds before being exposed to a water dose, some desorption of TMA may occur. However, this desorption time is usually small compared to the infiltration time and is assumed reasonably negligible. As highlighted in Figure 3d, the saturation value for this mass uptake at long times divided by the process pressure should be proportional to the solubility coefficient (S) of the TMA in PMMA at that process temperature. The temporal dependence of the mass uptake data at short times can be fit to **Equation 6** to extract an independent value for the effective diffusivity. Here we find the diffusivity at 70 °C to be $8.3\text{x}10^{-15}$ cm^2/s, similar to the value calculated with SIMS.

In Figure 4a, we plot representative film swelling data collected at three different VPI process temperatures. Immediately evident is that as process temperature is increased, maximum film swelling decreases. We further qualitatively confirmed this difference in inorganic loading at varying VPI process temperatures by burning off the polymer and measuring the thickness of the remaining oxide film (Fig. S6). This temperature dependent change in maximum sorption concentration can be used to evaluate the enthalpy of sorption (ΔH_s). Figure 4b plots the log of the solubility parameters for TMA in PMMA as a function of inverse temperature (Van't Hoff plot). These values were calculated by assuming that the concentration of TMA is a direct function of the swelling percentage. Because sorption capacity decreases with increasing process temperature, the overall sorption process must be exothermic. This exothermic behavior is consistent with usual measurements of sorption enthalpies of gases in polymers for membrane separations and can be generally attributed to the large exothermic enthalpy of condensation.[20, 29] Fig. 4b also indicates a change in the sorption enthalpy above and below 95 °C. Below 95 °C the ΔH_s is near zero (-0.03 eV). Above 95 °C, sorption enthalpy increases in magnitude to -0.33 eV (-31.8 kJ/mol).

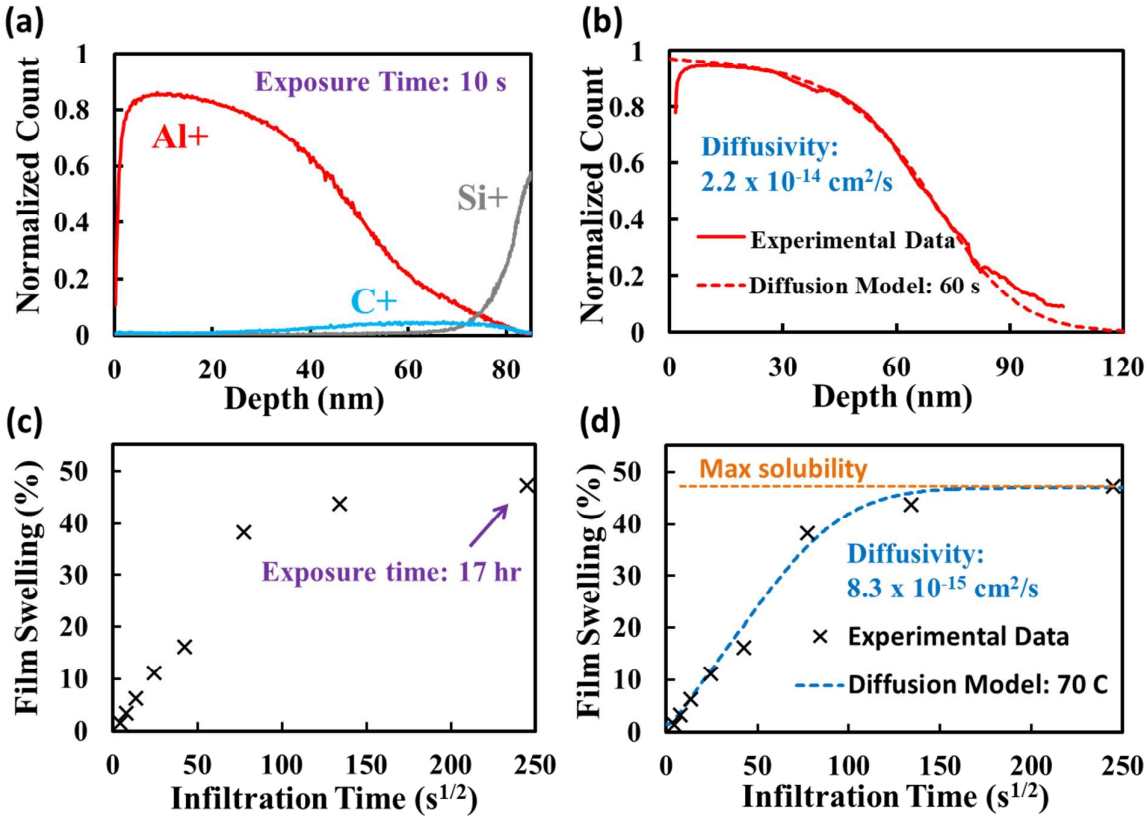

Figure 3: (a) SIMS data for Al+, Si+, and C+ signals as a function of depth into an initially 80 nm thick PMMA film treated with TMA VPI for 10 s at 70 °C. Concentration data is normalized to the total ion counts. (b) Fick's 2nd Law fit to the Al+ SIMS concentration profile for a PMMA film treated with TMA VPI at 70 °C for 60 s. Concentration data is normalized to the total ion counts. (c) Swelling data for an originally 150 nm thick PMMA film treated with TMA VPI at 70 °C. (d) Swelling data with fitted diffusion model and maximum solubility limit.

Figure 5 plots the natural log of the effective diffusivity measured with both SIMS and ellipsometry as a function of inverse temperature for TMA VPI of PMMA over a process temperature range of 60 °C to 130 °C. These measurements agree well with one another, providing us confidence in our accuracy. Again, a distinct change in linear slope occurs at 95 °C. Below 95 °C the effective activation energy for diffusion is 0.8 eV while above 95 °C the effective activation energy for diffusion is 2.2 eV. A full list of these measured effective diffusivities as a function of temperature is provided in Table 1.

5. Discussion:

Perspective with Respect to Prior Work and a Critical Process Temperature

Prior research has used *in situ* FTIR to explore the chemical mechanisms of the TMA-PMMA VPI process.[26, 28] These studies have revealed noticeable differences in precursor-polymer "reactivity" above and below 100 °C, near the temperature that we measure abrupt changes in the enthalpies associated with solubility and diffusion for this system. Using *ex situ* FTIR (Figure S7 in the SI), we have confirmed similar reactions in our own material above this critical temperature. The prior *in situ* FTIR studies of the TMA-PMMA VPI process have suggested that below ~100 °C, quasi-stable complexes form between the precursor and the polymer. At these low temperatures, this complex formation is reversible, and TMA can fully desorb from the PMMA if given sufficient time to do so. Above 100 °C, *in situ* FTIR studies have detected the onset of a permanent chemical reaction that occurs "quickly" between the TMA and PMMA.

Here, we propose the following atomic-scale physiochemical mechanisms to better understand the VPI processing in this precursor-polymer system. First, we note that the changes in both the solubility parameter and diffusion mechanism occur at 95 °C or about 10 °C below the expected glass transition temperature of our PMMA (T_g of 105 °C according to the source vendor, Sigma-Aldrich. See SI where we further confirm this T_g using temperature dependent ellipsometric measurements of a pure PMMA film). This difference in temperature may indicate that these changes in physiochemical mechanism are unrelated to the glass transition and simply the result of reactions. However, the

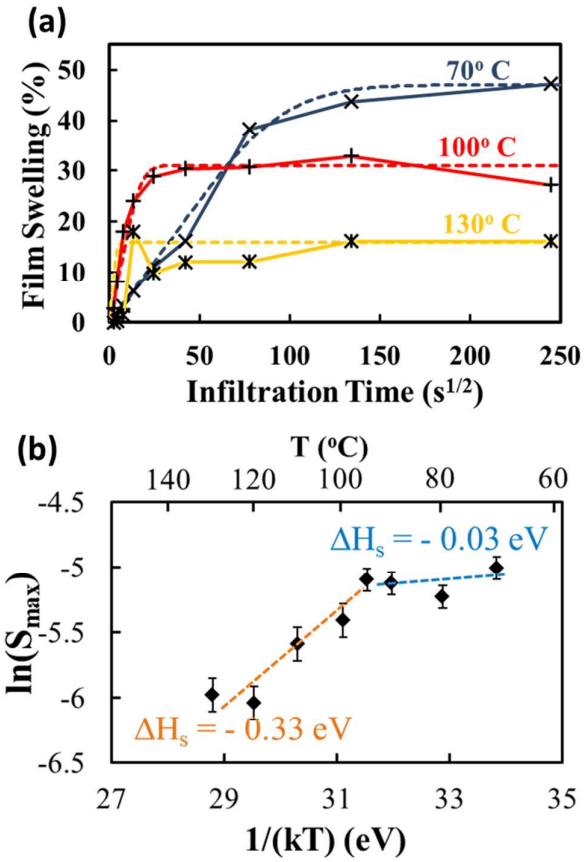

Figure 4: *(a) Plot of PMMA film swelling as a function of TMA VPI process time at three representative process temperatures: 70 °C, 100 °C, 130 °C. Dotted lines are regression fits to Fick's 2nd Law. (b) Van't Hoff plot of the maximum TMA solubility in PMMA as a function of VPI process temperature. Trend lines are added to visually indicate the change in sorption enthalpy at approximately 95 °C.*

proximity to the glass transition temperature and the well-known mechanistic changes that occur for small molecule sorption and diffusion above and below the glass transition temperature in other systems like gas diffusion membranes[21, 30, 31] make us suspect that TMA is acting as a plasticizer for PMMA and effectively lowering its T_g to 95 °C. While direct measurements of the glass transition for this system, like differential scanning calorimetry, are difficult because of TMA's reactivity, many small molecules with alkyl groups are known to plasticize PMMA, like methane, alcohols, and alkanes.[32-34]

In the following sections, we provide mechanistic descriptions that include explanations for changes in observed behavior based upon this critical temperature (95 °C) possibly representing the glassy-to-rubbery structural change in PMMA in a TMA atmosphere.

Precursor Sorption

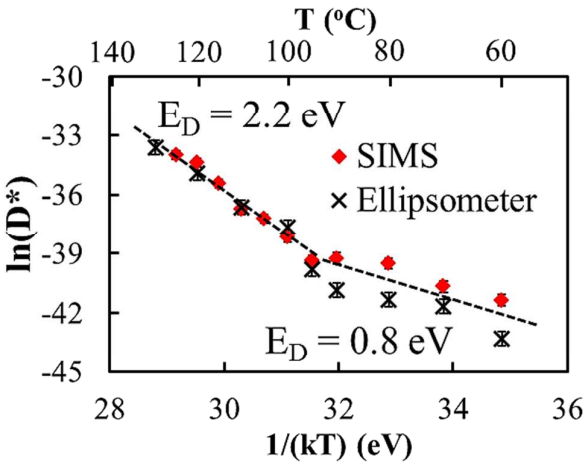

Figure 5: *Arrhenius plot of the effective diffusivity of TMA in PMMA as a function of VPI process temperature. Diffusivity data derived from both SIMS (red diamonds) and ellipsometry analyses (black x's) are included. Activation energies based on the slopes of the linear sections are reported. Linear regression fits (dotted lines) are added to visually emphasize the change in mechanism at about 95 °C.*

In the Van't Hoff plot for VPI sorption equilibrium (Figure 4b), we note a change in the sorption reaction mechanism above and below the critical process temperature of 95 °C. Specifically, the high-temperature (possibly rubbery) state has a more exothermic enthalpy of sorption (-0.33 eV) than the low temperature (possibly glassy) state (-0.03 eV). To better understand these enthalpies, it is useful to further partition this energy into several potential terms:[35]

$$\Delta H_S = \Delta H_{condensation} + \Delta H_{mix} \quad \textbf{Equation 15}$$

The first term ($\Delta H_{condensation}$) is the condensation of the vapor to the condensed state. While the exact nature of this term is not fully agreed upon (it may be some form of a gas adsorption energy rather than the gas-to-liquid latent heat), it is certainly exothermic in nature and the primary reason for why the Van't Hoff slopes are usually positive for gas sorption equilibria. The second term, the enthalpy of mixing (ΔH_{mix}), can be endothermic or exothermic depending on the penetrant-polymer interaction energy (i.e., related to the χ parameter).

The Van't Hoff data in Figure 4b is substantially different from what is typically observed for small molecule (e.g., H_2O, CO_2, N_2, etc.) sorption in polymers.[20] In more commonly studied gas sorption systems, the ΔH_s is usually observed to become more endothermic above the glass transition temperature. This endothermic change in enthalpy is attributed to the loss of free volume, which makes gas molecule sorption energetically less favorable (the dual-mode sorption model) – only solution sorption remains active.[18, 20] Here, we observe the rubbery state to have a significantly more exothermic ΔH_s than the glassy state. We interpret this change in enthalpy as an indication of a change in the enthalpy of mixing (ΔH_{mix}) due to the formation of the organic-inorganic

Temperature (°C)	D_{SIMS}^{*} (cm^2/s)	$D_{Ellipsometry}^{*}$ (cm^2/s)
60	1.1×10^{-14}	1.6×10^{-15}
70	2.2×10^{-14}	8.3×10^{-15}
80	7.0×10^{-14}	1.2×10^{-14}
90	9.0×10^{-14}	1.9×10^{-14}
95	8.0×10^{-14}	5.2×10^{-14}
100	2.6×10^{-13}	4.4×10^{-13}
105	7.0×10^{-13}	-
110	1.1×10^{-12}	1.2×10^{-12}
115	4.0×10^{-12}	-
120	1.2×10^{-11}	7.0×10^{-12}
125	1.7×10^{-11}	-
130	-	2.5×10^{-11}

***Table 1**: Summary of the effective diffusion coefficients measured for TMA VPI of PMMA calculated from SIMS and ellipsometry data at various process temperatures.*

hybrid material. Unlike most commonly studied gas-polymer sorption systems, VPI processing uses gases that can react with the polymer and change its inherent chemistry. Thus, we believe the sudden exothermic change in sorption enthalpy above T_g is indicative of the precursor molecule reacting with the polymer, creating a hybrid material that better mixes with TMA.

A second, more subtle, observation is the rather low exothermic value for the enthalpy of sorption for TMA in the glassy PMMA polymer (-0.03 eV). Most small gas molecule sorption enthalpies into glassy polymers are within the -0.1 to -0.3 eV range.[20] For example, CO_2 in PMMA has been measured to be -0.16 eV.[19] The low ΔH_s observed for this VPI process suggests the inclusion of another endothermic sub-process occurring upon TMA sorption. We propose this endothermic sub-process to be the de-dimerization of the TMA. Within our VPI process temperature range (< 140 °C), most of the vapor phase TMA is expected to be dimerized.[36] Consequently, as depicted in Figure 6, we propose describing the sorption of TMA into PMMA by three distinct steps: (1) condensation of the TMA vapor onto the PMMA surface, (2) dissociation of the dimerized TMA into individual TMA molecules, (3) dissolution (enthalpy of mixing) of the TMA into the PMMA:

$$\Delta H_S = \Delta H_{condensation} + \Delta H_{mix} + \Delta H_{dissociation}$$

Equation 16

Based on the above discussion, we attempt to further quantify the energies associated with these sorption sub-processes. From the literature, the enthalpy for condensation of TMA in dimer form is approximately -0.42 eV (exothermic),[37] and the enthalpy for TMA dimer dissociation is +0.87 eV (endothermic)[36]. Accounting for the reaction stoichiometry (see SI for details), we can then use Equation 16

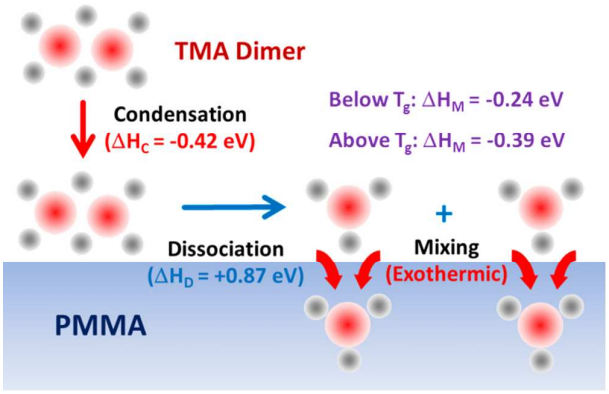

***Figure 6:** Schematic of TMA sorption into PMMA assuming dimer dissociation. Exothermic processes are labeled in red, and endothermic processes are labeled in blue.*

to estimate that the enthalpy of mixing for TMA-PMMA to be -0.24 eV (single TMA) in the glassy state and -0.39 eV (single TMA) in the rubbery state. We caveat these derived values by re-emphasizing the assumptions made herein: (1) solution behavior is sufficiently dilute to follow Henry's Law, (2) the TMA sorbs dissociated, not as a dimer, and (3) the condensation step can be approximated from the latent heat of fusion.

Precursor Diffusion and Reaction

The diffusional and reaction processes that occur during VPI can be explored using the Arrhenius plot presented in Figure 5. Here, we plot the natural log of diffusivity versus inverse temperature. A change in the Arrhenius slope is again observed at the critical process temperature of 95 °C. At low temperatures (possibly glassy PMMA), the Arrhenius slope (-0.8 eV) can be solely attributed to the activation barrier for TMA diffusion in PMMA, i.e., +0.8 eV (endothermic). Berens and Hopfenberg measured activation energies for diffusion of small molecules of similar size to TMA in PMMA between 30 °C and 90 °C to lie between 0.6 and 1.3 eV, comparable to our measurements.[22] At higher temperatures, the Arrhenius slope increases to -2.2 eV. We propose this increase to be a combination of the diffusional activation energy and the TMA-PMMA reaction enthalpy, as described by Equation 14, which illustrates that a reaction sink will create an effectively "slower" diffusion rate. Assuming the activation energy for true solution diffusion (ΔH_D) is the same above and below the 95 °C critical temperature, the TMA-PMMA reaction energy (ΔH_{rxn}) is found to be a reasonable exothermic value of -1.4 eV. If this critical temperature does represent the polymer's glassy-to-rubbery transition, then this change in state may explain the observed change in "reaction attempt frequency". Note that the linear intercepts for the Arrhenius plot (Figure 5) are equal to D_o^*, which is proportional to the "attempt frequency" for a given process. Above the glass transition temperature, more polymer chain motion is expected, and hence, an increase in the Arrhenius intercept (reaction attempt frequency) would occur as observed.

An alternative interpretation of this Arrhenius plot is that the activation energy for diffusion is smaller below the glass transition temperature because of the increase in free volume. Small molecules are known to more easily diffuse through the free volume of a glassy polymer than via solution diffusion in a rubbery polymer.[21] However, because our Van't Hoff plot shows the opposite trend from standard gas sorption, it suggests that the dimerized TMA is not directly accessing the free volume of the polymer. Rather, only solution diffusion mechanisms are presumed active. Furthermore, *in situ* FTIR studies confirm the onset of a permanent chemical reaction between TMA and PMMA near 95°C.[27, 28] Thus, we believe that the onset of a diffusion-reaction mechanism above 95°C is more likely than a change in the polymer's diffusional energy barrier alone.

A final consideration to be noted is that these measurements include both the TMA molecule uptake process as well as the sorption and reaction of water molecules. Using *ex situ* measurements, as done here, we cannot deconvolute these two processes, and it is likely prudent to further explore these mechanisms via *in situ* methods. However, our approach to analyzing these physiochemical kinetics are still valid and representative for the entire process and have value for materials design as demonstrated in the next section.

Practical Implementation of Rational VPI Process Design

While understanding the atomistic scale mechanisms of VPI sorption, transport, and reaction will be important to developing intuitive predictions about the expected behavior of new precursor-polymer couples, understanding these mechanisms is not important if one simply wants to apply rational design principles for controlling the mass uptake and infiltration depth. To achieve this rational design, one simply needs to measure the ΔH_s and ΔH_{D^*} and the pre-exponential factors as done in this paper. These values can then be used to calculate solubility and diffusivity at any temperature and substituted into the solution for Fick's 2nd Law for any geometry.

To demonstrate this level of rational design, we have calculated the process time required to infiltrate a 1.4 micron PMMA film on an impermeable substrate to a depth of 400 nm. Based on the energy parameters reported above, we estimate a process time of 10 min at 100 °C. (See calculations in the SI.) In Figure 7, we show a cross-sectional SEM micrograph of this VPI infiltrated film. The yellow line at the right of Figure 7 is the EDX line scan of the aluminum signal across the film. The infiltrated region is slightly brighter due to higher atomic number contract, but this layer is essentially homogeneous at the atomic scale (no indication of aggregated Al_2O_3 secondary phases). The EDX line scan shows aluminum concentrated in the top third of the film cross section, or about 400 nm, which is close to our prediction, demonstrating the ability to use these fundamental parameters to help design future VPI processes.

Conclusions

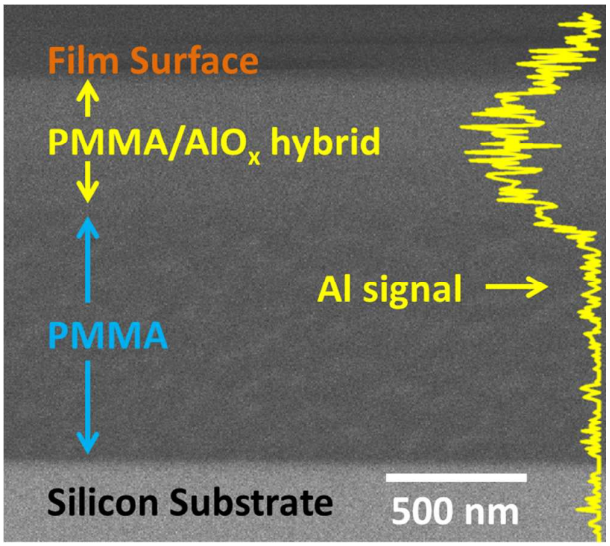

***Figure 7**: SEM image with EDX line scan on a 1.4 micron PMMA film infiltrated with TMA at 100 °C for 10 minutes.*

This work has developed a phenomenological theory and an experimental approach for measuring the fundamental energy parameters associated with the processing kinetics for vapor phase infiltration. Once these fundamental energy parameters are known, VPI processes can be rationally designed (e.g., process temperatures and times) to achieve desired infiltration depth and inorganic loading fraction for any given starting polymer geometry (film, fiber, etc.). Measurements of the vapor precursor's equilibrium solubility as a function of temperature can be fit to a Van't Hoff equation to assess the thermodynamic enthalpy of sorption in the polymer host. Measurements of the penetrant's diffusivity as a function of temperature can be used to determine the activation energy for diffusion and potentially detect changes in the rate-limiting mechanism. Here we find that the TMA-PMMA model system changes both its solubility enthalpy and diffusional activation energy near the glass transition temperature of the polymer. We ascribe these changes to greater polymer chain motion, which accelerates reaction kinetics. The resulting organic-inorganic hybrid material is then more soluble towards the TMA precursor. While the phenomenological theory for VPI processing kinetics developed herein can be used for quantitative materials design, continued research with complementary characterization techniques and *ab initio* simulations will be needed to fully understand and predict the atomic-scale mechanisms occurring in new precursor-polymer couple VPI chemistries.

Conflicts of interest

There are no conflicts to declare.

Acknowledgments:

Acknowledgment is made to the donors of the American Chemical Society Petroleum Research Fund for support of this research – Grant # 55526-DNI10. This work was performed in part at the Georgia Tech Institute for Electronics and Nanotechnology, a member of the National Nanotechnology Coordinated Infrastructure, which is supported by the National Science Foundation (Grant ECCS-1542174). The authors would also like to thank Professors Ryan Lively and William Koros for insightful discussions about gas molecule sorption processes in polymers.

References

1. C. Z. Leng and M. D. Losego, *Mater Horiz*, 2017, **4**, 747-771.
2. M. Ramanathan, Y. C. Tseng, K. Ariga and S. B. Darling, *J Mater Chem C*, 2013, **1**, 2080-2091.
3. S. M. Lee, E. Pippel, U. Gosele, C. Dresbach, Y. Qin, C. V. Chandran, T. Brauniger, G. Hause and M. Knez, *Science*, 2009, **324**, 488-492.
4. B. Gong, J. C. Spagnola and G. N. Parsons, *J Vac Sci Technol A*, 2012, **30**.
5. S. Obuchovsky, I. Deckman, M. Moshonov, T. S. Peretz, G. Ankonina, T. J. Savenije and G. L. Frey, *J Mater Chem C*, 2014, **2**, 8903-8910.
6. C. D. McClure, C. J. Oldham and G. N. Parsons, *Surf Coat Tech*, 2015, **261**, 411-417.
7. T. Segal-Peretz, J. Winterstein, M. Doxastakis, A. Ramirez-Hernandez, M. Biswas, J. X. Ren, H. S. Suh, S. B. Darling, J. A. Liddle, J. W. Elam, J. J. de Pablo, N. J. Zaluzec and P. F. Nealey, *Acs Nano*, 2015, **9**, 5333-5347.
8. W. K. Wang, F. Yang, C. Q. Chen, L. B. Zhang, Y. Qin and M. Knez, *Adv Mater Interfaces*, 2017, **4**.
9. H. I. Akyildiz, K. L. Stano, A. T. Roberts, H. O. Everitt and J. S. Jur, *Langmuir*, 2016, **32**, 4289-4296.
10. H. I. Akyildiz, M. Lo, E. Dillon, A. T. Roberts, H. O. Everitt and J. S. Jur, *J Mater Res*, 2014, **29**, 2817-2826.
11. C. Y. Nam, A. Stein and K. Kisslinger, *J Vac Sci Technol B*, 2015, **33**.
12. S. Obuchovsky, B. Shamieh, I. Deckman, G. Ankonina and G. L. Frey, *Sol Energ Mat Sol C*, 2015, **143**, 280-283.
13. Y. C. Tseng, Q. Peng, L. E. Ocola, D. A. Czaplewski, J. W. Elam and S. B. Darling, *J Vac Sci Technol B*, 2011, **29**.
14. W. K. Wang, C. Q. Chen, C. Tollan, F. Yang, Y. Qin and M. Knez, *J Mater Chem C*, 2017, **5**, 2686-2694.
15. Y. H. Yu, Z. D. Li, Y. M. Wang, S. Q. Gong and X. D. Wang, *Adv Mater*, 2015, **27**, 4938-4944.
16. D. Berman, S. Guha, B. Lee, J. W. Elam, S. B. Darling and E. V. Shevchenko, *Acs Nano*, 2017, **11**, 2521-2530.
17. E. Barry, A. U. Mane, J. A. Libera, J. W. Elam and S. B. Darling, *J Mater Chem A*, 2017, **5**, 2929-2935.
18. W. J. Koros and D. R. Paul, *J Polym Sci Pol Phys*, 1978, **16**, 1947-1963.
19. W. J. Koros, G. N. Smith and V. Stannett, *J Appl Polym Sci*, 1981, **26**, 159-170.
20. A. S. Michaels, J. A. Barrie and W. R. Vieth, *J Appl Phys*, 1963, **34**, 1-12.
21. N. Ramesh, P. K. Davis, J. M. Zielinski, R. P. Danner and J. L. Duda, *J Polym Sci Pol Phys*, 2011, **49**, 1629-1644.
22. A. R. Berens and H. B. Hopfenberg, *J Membrane Sci*, 1982, **10**, 283-303.
23. A. Sinha, D. W. Hess and C. L. Henderson, *J Vac Sci Technol B*, 2007, **25**, 1721-1728.
24. Q. Peng, Y. C. Tseng, Y. Long, A. U. Mane, S. DiDona, S. B. Darling and J. W. Elam, *Langmuir*, 2017, **33**, 13214-13223.
25. J. Crank, *The Mathematics of Diffusion*, Clarendon Press, Oxford, Eng, 2d edn., 1975.
26. M. Biswas, J. A. Libera, S. B. Darling and J. W. Elam, *Chem Mater*, 2014, **26**, 6135-6141.
27. M. Biswas, J. A. Libera, S. B. Darling and J. W. Elam, *J Phys Chem C*, 2015, **119**, 14585-14592.
28. E. C. Dandley, C. D. Needham, P. S. Williams, A. H. Brozena, C. J. Oldham and G. N. Parsons, *J Mater Chem C*, 2014, **2**, 9416-9424.
29. P. Meares, *J Am Chem Soc*, 1954, **76**, 3415-3422.
30. H. Y. Kaptan, *J Appl Polym Sci*, 1999, **71**, 1203-1207.
31. I. H. Romdhane, R. P. Danner and J. L. Duda, *Ind Eng Chem Res*, 1995, **34**, 2833-2840.
32. J. M. G. Cowie, M. A. Mohsin and I. J. Mcewen, *Polymer*, 1987, **28**, 1569-1572.
33. Y. P. Handa, P. Kruus and M. ONeill, *J Polym Sci Pol Phys*, 1996, **34**, 2635-2639.
34. S. S. Li, J. L. Shen and A. E. Tonelli, *Polymer*, 2018, **135**, 355-361.
35. A. Ghadimi, S. Norouzbahari and T. Mohammadi, *J Chem Eng Data*, 2017, **62**, 1433-1439.
36. A. W. Laubengayer and W. F. Gilliam, *J Am Chem Soc*, 1941, **63**, 477-479.
37. J. P. McCullough, J. F. Messerly, R. T. Moore and S. S. Todd, *The Journal of Physical Chemistry*, 1963, **67**, 677-679.

Table of Contents Graphic:

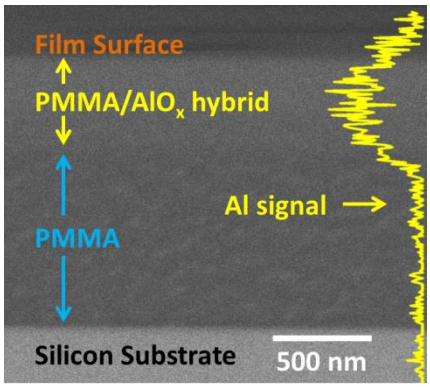

We develop and apply a kinetics model for vapor phase infiltration to precisely control polymer transformation by metalorganic precursors.